Quercetin 3-O-glucuronide-rich Lotus Leaf Extract Promotes a Brown-fat-phenotype in $C_3H_{10}T_{1/2}$ Mesenchymal Stem Cells

Zhenyu Wang[a,b], Chaoyi Xue[a,b], Xuan Wang[a,b], Maomao Zeng[a,b], Zhaojun Wang[a,b], Qiuming Chen[a,b], Jie Chen[a,b], Mark Christian[*,c], and Zhiyong He[*, a,b]

[a]State Key Laboratory of Food Science and Technology, Jiangnan University, Wuxi, Jiangsu 214122, China

[b]International Joint Laboratory on Food Safety, Jiangnan University, Wuxi, Jiangsu 214122, China

[c]School of Science and Technology, Nottingham Trent University, Clifton, Nottingham, NG11 8NS, United Kingdom

[*]Corresponding author. Tel: +86 510 8591 9065; fax: +86 510 8591 9065.

E-mail address: zyhe@jiangnan.edu.cn (He Z.), mark.christian@ntu.ac.uk (M. Christian)

Abstract

Lotus (*Nelumbo nucifera G*aertn.) is an aquatic perennial crop planted worldwide and its leaf (also called "He-Ye") has therapeutic effects on obesity. However, whether the underlying mechanism leads to increased energy expenditure by activation of brown adipocytes has not been clarified. Here, murine $C_3H_{10}T_{1/2}$ mesenchymal stem cells (MSCs) were employed to investigate the effects of ethanol extracts from lotus leaf (LLE) on brown adipocytes formation and the underlying molecular mechanisms. The results showed LLE was rich in polyphenols (383.7 mg/g) and flavonoids (178.3 mg/g), with quercetin 3-O-glucuronide (Q3G) the most abundant (128.2 μg/mg). In LLE-treated $C_3H_{10}T_{1/2}$ MSCs, the expressions of lipolytic factors (e.g., ATGL, HSL, and ABHD5) and brown regulators (e.g., Sirt1, PGC-1α, Cidea, and UCP1) were significantly upregulated compared to that in the untreated MSCs. Furthermore, LLE promoted mitochondrial biogenesis and fatty acid β-oxidation, as evidenced by increases in the expression of Tfam, Cox7A, CoxIV, Cox2, Pparα, and Adrb3. Likewise, enhanced browning and mitochondrial biogenesis were also observed in Q3G-stimulated cells. Importantly, LLE and Q3G induced phosphorylation of AMPK accompanied by a remarkable increase in the brown fat marker UCP1, while pretreatment with Compound C (an AMPK inhibitor) reversed these changes. Moreover, stimulating LLE or Q3G-treated cells with CL316243 (a beta3-AR agonist) increased p-AMPKα/AMPKα ratio and UCP1 protein expression, indicating β3-AR/AMPK signaling may involve in this process. Collectively, these observations suggested that LLE, especially the component Q3G, stimulates thermogenesis by activating brown adipocytes, which may involve the β3-AR/AMPK signaling pathway.

Keywords: Lotus leaf extracts, Quercetin-3-O-glucuronide, Brown adipocyte, Mitochondrial biogenesis, AMPK

1. Introduction

Obesity occurs when the intake of calories exceeds the expenditure of energy, and it results in significant health problems, including insulin resistance, diabetes, and nonalcoholic fatty liver disease (Sharma et al., 2019). It is characterised by increased size (hypertrophy) and number (hyperplasia) of adipocytes, resulting in an abnormal amount of fat mass (Wang et al., 2019). Based on the origin, morphology and function, adipocytes can be classified into three types: white, brown, and beige/brite (Giralt & Villarroya, 2013). Functionally speaking, white adipocytes are responsible for triglyceride storage while brown or beige adipocytes possess multilocular lipid droplets and uncoupling protein 1 (UCP1)-rich mitochondria, which burn lipids to produce heat (Chou, Ho, & Pan, 2018; S. Wang, Pan, Hung, Tung, & Ho, 2019). Several critical regulators are implicated in the differentiation and activation of brown adipocytes, such as CCAAT enhancer-binding protein α (C/EBPα), peroxisome proliferator-activated receptor γ (PPARγ), PR domain-containing 16 (PRDM16), and PPAR γ coactivator-1α (PGC-1α) (Hu, Wang, Tan, & Christian, 2020).

Therefore, the recruitment of brown adipocytes is being positioned as a prospective therapy for treating obesity and associated metabolic abnormalities. Currently, external factors (e.g., cold exposure, exercise and intermittent fasting) and pharmacological factors (e.g., indomethacin, isoproterenol, lobeglitazone, and sitagliptin) have been proposed as inducers of brown adipose tissue (BAT) activation and thermogenesis (Wang, Zeng, et al., 2021). However, the associated

therapies are either impractical (e.g., cold) or may cause undesirable side effects once the dose exceeds physiological levels (e.g., thyroid) (Enerbäck, 2010). The search for natural phytochemicals, including polyphenols, alkaloids, terpenoids, n-3 polyunsaturated fatty acids, saponins, and phytosterols, has received increasing interest and is considered a prospective strategy for the recruitment of BAT (Wang et al., 2021b).

Lotus (*Nelumbo nucifera* Gaertn.), an aquatic perennial crop belonging to the family of Nelumbonaceae, has been cultivated in Asia (China, Japan, India and other Southeast Asian countries), the Americas, and Oceania for thousands of years. As an important part of the lotus plant, lotus leaves have been used as medicinal purposes for a long time due to their rich content of beneficial compounds, including polyphenols (e.g., kaempferol and quercetin derivatives), polysaccharides, alkaloids (e.g., nuciferine, N-nornuciferine, pronuciferine), steroids and saponins (Limwachiranon, Huang, Shi, Li, & Luo, 2018; Wang et al., 2021a). Compelling evidence from multiple epidemiological and laboratory surveys supports the positive correlation between regular lotus leaves intake and weight loss. The potential mechanisms are as follows:1) inhibition of lipase activity in the intestinal absorption phase, thus reducing the hydrolysis and absorption of fat by the body. 2) reduction of lipid synthesis, enhancement of lipid oxidation metabolism, and increase of lipoproteinase and hepatic lipase activity in the utilization phase of the body, thus preventing fat accumulation (Wang et al., 2021a). In general, investigations of the anti-obesity effects of lotus leaves has mainly targeted the liver and white adipose tissue (WAT), while its effect on expenditure (thermogenesis) by acting on brown fat is not well understood. Emerging evidence suggests lotus leaves promote lipid metabolism by

85 greatly upregulating *Pparα* (a factor responsible for mitochondrial oxidation) and *Ucp2* (a
86 factor involved in mitochondrial respiration) in the epididymal WAT of obese mice (Sim et al.,
87 2019). Moreover, another investigation from Song and collaborators demonstrated that
88 mixtures of lotus leaves and *P. persica* flowers (43:57) markedly enhance the mRNA
89 expression of *Ppargc1a* and *Pparα* in mesenteric WAT of HFD-fed mice, therefore favoring
90 fatty acid oxidation (Song, Kim, Park, & Kim, 2020). Therefore, these results (increase in the
91 mRNA expression of *Ppargc1a* , *Pparα, Ucp2*) led us to speculate that ethanol extracts from
92 lotus leaf (LLE) may mediate brown-fat formation and activity by inducing some critical
93 regulators. Importantly, AMP-activated protein kinase (AMPK), a main modulator of energy
94 metabolism, induces mitochondrial biogenesis and thermogenesis by uncoupling UCP1 in BAT
95 (van der Vaart, Boon, & Houtkooper, 2021). $C_3H_{10}T_{1/2}$ mesenchymal stem cells (MSCs) are
96 considered to be an ideal model for establishing brown adipocytes with the potential to
97 differentiate into mature brown adipocytes upon stimulatory induction of hormones (Imran et
98 al., 2017; Rahman & Kim, 2020b; Wang et al., 2018). To verify whether lotus leaves possess a
99 brown-promoting ability, the effects of ethanol extracts from lotus leaf (LLE) on brown
100 remodelling in $C_3H_{10}T_{1/2}$ cells and the involvement of AMPK pathway activation in this effect
101 were investigated.
102
103 **2. Materials and Methods**
104 **2.1 Materials**
105 Murine $C_3H_{10}T_{1/2}$ MSCs were purchased from the Cell Bank of the Chinese Academy of

106 Sciences (Kunming, China). 1-Methyl-3-isobutylxanthine (IBMX), indomethacin (Indo), and
107 rosiglitazone (Ros), dexamethasone (Dex), triiodothyronine (T_3) and insulin (Ins) were
108 purchased from Macklin (Shanghai, China). Forskolin, dorsomorphin (Compound C), and
109 CL316243 were purchased from MCE (Medchem Express, USA).

110 **2.2. Preparation of LLE**

111 A total of 50 g of dried lotus leaves (Bozhou, Anhui, China) was stirred in 750 mL of 80%
112 ethanol for 1.5 h, including sonication pretreatment for 0.5 h (44 KHz, 55% power) at room
113 temperature. The extraction solutions were obtained by filtration (slow filter paper, 90 cm
114 Sinopharm Group Co. Ltd.) and further concentrated using a rotary evaporator (Buchi,
115 Switzerland) at 40 °C. The concentrated LLE was lyophilised and stored at -20 °C until use.

116 **2.3. Components of LLE**

117 **2.3.1. Total polyphenol content determination**

118 The content of total polyphenol (TPC) in LLE was measured with a microplate reader
119 (Spectramax190, Molecular Devices, USA) using gallic acid as a standard. The optical density
120 was measured at 725 nm, as we previously reported (Cheng et al., 2021). The standard curve
121 is $Y=0.0011X+0.043$ ($R^2=0.9999$) (Y is the optical density (OD_{725}) and X is the concentration
122 of gallic acid in μg/mL).

123 **2.3.2. Total flavonoid content determination**

124 The content of total flavonoid (TFC) in LLE was measured with a microplate reader
125 (Spectramax190, Molecular Devices, USA) using rutin as a standard. The optical density was
126 measured at 725 nm, as we previously reported (Cheng et al., 2021). The standard curve is

127 Y=2.9099X+0.0315 (R^2=0.9945) (Y is the optical density (OD_{510}) and X is the concentration
128 of rutin in μg/mL).

129 **2.3.3. Polysaccharide content determination**

130 The polysaccharide content in LLE was measured with the phenolsulfuric acid method using
131 glucose as a standard. The optical density was read at 490 nm, as described by Sanhueza and
132 collaborators (Sanhueza, Paredes-Osses, González, & García, 2015). The standard curve is
133 Y=0.0173X+0.0374 (R^2=0.9928) (Y is the optical density (OD_{490}) and X is the concentration
134 of glucose in μg/mL)

135 **2.3.4. Protein content determination**

136 The protein content in LLE were measured employing Kjeldahl method according to GB/T
137 5009.5-2003. The Kjeldahl Nitrogen amount of LLE was firstly determined and then a
138 conversion factor of 6.25 was used to calculate the protein content.

139 **2.3.5. Phenolic compounds analysis**

140 The phenolic compounds in LLE were analysed by UPLC-QTOF-MS (MALDI SYNAPT MS,
141 USA) methods in accordance with previous reports from our laboratory (Wu et al., 2022).
142 Masslynx 4.1 software (Waters Corporation, Milford, MA) was used for the analysis of MS
143 data.

144 **2.4. Cell culture, differentiation, and treatment**

145 $C_3H_{10}T_{1/2}$ cells were maintained in DMEM (Gibco, US) with 10% fetal bovine serum (FBS)
146 (Lonsera, Uruguay) and 1% penicillin/streptomycin (BioSharp, China) at 37 °C in a 5% CO_2
147 environment. The induction programme of $C_3H_{10}T_{1/2}$ cells into brown adipocytes was

148 performed as previously reported (Yue et al., 2019; Zhang et al., 2014). Briefly, confluent cells
149 were treated with DMEM containing 10% FBS, 0.5 mM IBMX, 125 nM Indo, 1 mM Dex, 850
150 nM Ins, 1 nM T_3 and 1 mM Ros for 2 days before the induced medium was changed to
151 differentiation medium (850 nM Ins, 1 nM T_3, and 1 mM Ros) for another 4 days. LLE (50,
152 100, and 200 μg/mL) or Q3G (1, 5, and 10 μM) (Yuanye, Shanghai, China) were added during
153 the stage of differentiation. For AMPK inhibition or β3-AR activation, the cells were incubated
154 with Compound C (Com C, 5 μM) or CL316243 (1μM) for 24 h, respectively, and then
155 collected.

156 **2.5. Cell Viability Assay**

157 The cytotoxicity of different samples on $C_3H_{10}T_{1/2}$ cells was determined using Cell Counting
158 Kit-8 (CCK-8) (Beyotime, Jiangsu, China) following our previous procedure (Wang et al.,
159 2019). Cells were treated with various concentrations of LLE (0-200 μg/mL) or Q3G for 24 or
160 48 h, then 10 μL of CCK-8 solution was infused and incubated at 37°C for 1 h, after which
161 absorbance was recorded at 450 nm using enzyme calibrator.

162 **2.6. BODIPY 505/515 lipid staining**

163 Cells were plated onto coverslips, differentiated for 6 days and then washed twice with PBS,
164 fixed in 4% paraformaldehyde, and incubated with BODIPY green (1 μM) (#GC42960,
165 GLPBIO, USA) for 15 min. Subsequently, the stained cells were washed twice with PBS,
166 incubated with DAPI (1 μg/mL) for 1 min, and then washed 3 more times with PBS. The
167 phenotypic changes were captured using an inverted fluorescence microscope (Axio Vert.A1,
168 Germany).

169 **2.7. Mitochondrial Staining**

170 The mitochondrial content of the adipocytes were assessed by staining with MitoTracker Green
171 (Beyotime, China). After the LLE treatment, the culture media was discarded and Mito-Tracker
172 Green staining solution prewarmed at 37 °C was added and incubated in a 37 °C incubator for
173 15 min. Then, the staining solution was removed and fresh cell culture medium was added.
174 Subsequent observations were made with an inverted fluorescence microscope (Axio Vert.A1,
175 Germany).

176 **2.8. Reactive oxygen species (ROS) assay**

177 The 6-well plate was supplemented with 1m of fluorescent probe DCFH-DA (10mM) and
178 incubated at 37°C for 20 min in a 37 °C incubator. Thereafter, the cells were washed to
179 adequately remove the DCFH-DA remaining outside the cells. Then, the green fluorescence in
180 the FITC field was imaged with an inverted microscope (Axio Vert.A1, Germany) and analysed
181 using Image J (reversed-phase).

182 **2.9. Mitochondrial membrane potential (MMP) staining**

183 The MMP was evaluated via JC-1 staining (Beyotime, China). After treatment with LLE,
184 $C_3H_{10}T_{1/2}$ cells were incubated with a JC-1 staining solution (1 ml) for 20 min at 37°C.
185 Subsequently, the cells were photographed using an inverted fluorescence microscope (Axio
186 Vert.A1, Germany). Monomers and aggregates are shown as green and red fluorescence,
187 respectively.

188 2.10. Oxygen consumption rate assay

189 A BBoxiProbe™ R01 kit (Bestbio, China) was used for the evaluation of oxygen consumption

190 rate. Briefly, 1) cells were cultured in a 96-well black plate and treated with LLE or Q3G for
191 48h; 2) the medium was refreshed and 4μl of oxygen fluorescent probe was added; 3) oxygen
192 blocking buffer (100μL) was inserted to prevent external oxygen; 4) the rate of oxygen
193 consumption at 60 min was analyzed with a fluorescent microplate reader (λex=462 nm,
194 λem=603 nm).

195 **2.11. Quantitative RT-PCR analysis**

196 After 6 days of induced differentiation, brown adipocytes were collected for RNA extraction
197 using a Total RNA Isolation Kit (Vazyme, Nanjing, China). 0.5-0.8 μg of RNA was reverse
198 transcribed to cDNA using Maxime RT Premix (Vazyme, Nanjing, China). Then, a qRT-PCR
199 assay was performed with the CFX96 real-time PCR detection system (Bio-Rad, USA) using
200 ChamQ Universal SYBR Master Mix (Vazyme, Nanjing, China). Target genes were
201 normalized to the β-actin gene, and their respective relative expression was analysed by the
202 $2^{-\Delta\Delta Ct}$ method. The primer sequences are listed in Table 2.

203 **2.12. Immunofluorescence**

204 The $C_3H_{10}T_{1/2}$ cells seeded on coverslips were fixed in 4% paraformaldehyde for 1 h followed
205 by permeabilization using 0.25% Triton X-100 (Solarbio, Beijing, China). After washing with
206 PBS, cells were blocked in PBST containing 1% BSA for 1 h, followed by overnight incubation
207 with rabbit primary antibodies against Sirt1 (1:100 dilution) and UCP1 (1:100 dilution) at 4°C.
208 Immediately afterwards the cells were washed with PBS, then incubated with FITC/Cy3-
209 conjugated goat anti-rabbit secondary antibody (1:200 dilution) for 1.5 h at 25 °C. The nuclei
210 was then stained with DAPI (Beyotime, China), and preparations were examined by a inverted

211 fluorescence microscope (Axio Vert.A1, Germany).

212 **2.13. Western blotting**

213 After the cells were lysed with RIPA buffer (Beyotime, Jiangsu, China), proteins were collected
214 and subjected to 10% SDS-PAGE. Thereafter, the proteins were transferred onto PVDF
215 membranes (Beyotime, China) by a semidry transfer instrument (Bio-Rad Trans-blot Turbo) at
216 100~400 mA (25 V) for 20-30 min. After blocking at room temperature for 1 h in western
217 blotting buffer (Beyotime, China), the membranes were probed with rabbit primary antibodies
218 (CST, MA) against (p)AMPKα/β1 and (p)ACC (1:1000, CST) as well as UCP1, Sirt1, PGC-
219 1α, Tfam, Cox-2, Cox IV, HSL, ADBH5, and Plin5 (1:1000, Proteintech). Secondary antibodies
220 (1:1000, Proteintech) coupled to horseradish peroxidase were then subjected to
221 chemiluminescence detection using ECL detection reagents (Beyotime, China).

222 **2.14. Statistical Analysis**

223 Data from individual experiments are presented as the means ± standard deviation (SD).
224 Statistical significance was calculated using one-way analysis of variance (ANOVA) with
225 Duncan's test using DPS Software (values with different letters indicate a significant difference
226 ($P < 0.05$)).

227

228 **3. Results**

229 **3.1. Components of LLE**

230 The TPC, TFC, polysaccharide, and protein in LLE were determined to be 383.7±10.7 mg/g
231 gallic acid equivalent, 178.3±2.0 mg/g rutin equivalent, 225.3±1.6 mg/g glucose equivalent,

232 and 67.3±1.4 mg/g, respectively. Then, UPLC with PDA was used to analyse the phenolics
233 profile in LLE (Fig. 1(1)). The components appeared at the peaks A, B, C, D, E, F, and H were
234 identified as procyanidin B2 (6.86±0.44 μg/mg), quercetin 3-O-arabinopyranosyl-(1→2)-
235 galactopyranoside (12.95±0.82 μg/mg), rutin (1.52±0.10 μg/mg), quercetin 3-O-glucuronide
236 (128.21±8.16 μg/mg), kaempferol 3-O-glucoside (5.48±0.35 μg/mg), isorhamnetin 3-O-
237 rutinoside (0.52±0.03 μg/mg), and isorhamnetin 3-O-glucoside (3.51±0.22 μg/mg),
238 respectively, by comparing their MS and MS^2 fragmentation ions, and previously reported data
239 in the literature (Fig. 1 and Table 1).

240 **3.2. Effects of LLE on the viability of $C_3H_{10}T_{1/2}$ cells**

241 As observed in Fig. 2A, the viability of LLE (concentrations below 200 μg/mL)-treated cells
242 was comparable to that of the untreated cells, implying that the LLE did not have a significant
243 cytotoxic effect below 200 μg/mL. In the following experiments, LLE at concentrations of 50-
244 200 μg/mL was used for cells treatment.

245 **3.3. LLE promotes lipolysis without affecting differentiation of $C_3H_{10}T_{1/2}$ cells**

246 The results of LLE on $C_3H_{10}T_{1/2}$ cells differentiation showed the main adipocyte marker *Fabp4*
247 (fatty acid binding protein 4) and *Pparγ* had no obvious change among the different groups
248 although *C/ebpα* was markedly elevated in LLE-treated cells (only at 200 μg/mL) (Fig. 2B).
249 Moreover, microscopic examination of the Bodipy staining and bright field showed the
250 potential of LLE to reduce lipid droplet number (Fig. 2C) and size (Fig. 2D) compared to the
251 control. These data prompted us to investigate the possibility that LLE affected lipolysis. It was
252 found LLE (especially at 100 and 200μg/mL) significantly induced Abhd5 (abhydrolase

253 domain Containing 5) and Atgl (adipose triglyceride lipase) expressions at gene and protein
254 levels (Fig. 2E-G). Here, we showed HSL (hormone-sensitive triglyceride lipase) protein level
255 increased while mRNA level remained unchanged, suggesting that HSL is regulated mainly at
256 the post-transcriptional level (Fig. 2E-G). Collectively, LLE increased the potential for
257 lipolysis, but in $C_3H_{10}T_{1/2}$ cells differentiation into adipocytes is maintained.

258 **3.4. LLE induced BAT-enriched genes in differentiated $C_3H_{10}T_{1/2}$ cells**

259 Lipolysis of intracellular lipid serves as a critical role in the physiological regulation of BAT;
260 thus, we next explored the specific brown characteristics in LLE-treated $C_3H_{10}T_{1/2}$ cells. As
261 shown in Fig. 3A, LLE dose-dependently augmented the mRNA expression of BAT-rich genes,
262 such as *Ucp1*, *Ppargc1a*, *Cideα*, *Sirt1* but not *Prdm16* in comparison to the untreated control.
263 Notably, the lipid droplet-associated gene *Plin5* that was upregulated with LLE treatment, is
264 considered a browning marker due to its much higher expression in brown compared to white
265 adipose tissue (Fig. 3A(6)). In addition, a dose-dependent increase in the expression of SIRT1
266 (Fig. 3B and 3D) and UCP1 (Fig. 3C and 3E) upon LLE treatment was confirmed by
267 immunostaining.

268 **3.5. LLE promoted mitochondrial biogenesis in differentiated $C_3H_{10}T_{1/2}$ cells**

269 Brown adipocytes possess high mitochondrial numbers required for thermogenic function.
270 Therefore, we examined mitochondrial biogenesis in following studies. As seen in Fig. 4A and
271 4B, the mitochondrial abundance in LLE-treated $C_3H_{10}T_{1/2}$ cells showed a dose-dependent
272 increase. Moreover, mitochondria are both the source and target of ROS and results showed
273 LLE stimulation dose-dependently lowered the ROS level (Fig. 4C and 4D). MMP is a critical

274 indicator of mitochondrial activity and the results revealed a significantly higher fluorescence
275 ratio in the LLE group than in the control (Fig. 4E and 4F). In addition, the enhanced oxygen
276 consumption rate was demonstrated in LLE-treated cells, which further confirm the potential
277 of LLE (Supplemental Fig. 1). To elucidate the mechanism underlying the effects of LLE on
278 mitochondrial activity in $C_3H_{10}T_{1/2}$ adipocytes, specific regulators involving mitochondrial
279 function were evaluated. The results showed that the mRNA and/or protein expression levels
280 of mitochondrial transcription factor A (TFAM) (Fig. 4G(1), and Fig. 4H and Fig. 4I(1)) and
281 nuclear respiratory factor 2 (NRF2) (Fig. 4H and Fig. 4I(4)) were dramatically increased by
282 LLE treatment, respectively, while *Nrf1* expression remained unchanged (Fig. 4G(2)).
283 Moreover, we also found that LLE treatment markedly elevated the expression of other
284 mitochondrial biogenesis-associated factors, including *Adrb3* (beta 3 adrenergic receptor, β3-
285 AR) (Fig. 4G(3)), *Pparα* (Fig. 4G(4)), cytochrome c oxidase subunit VII a (*Cox7a*) (Fig. 4G(5)),
286 COX-2 (Fig. 4G(6), Fig. 4H and Fig. 4I(2)), and COX-IV (Fig. 4H and Fig. 4I(3)). These results
287 revealed that LLE stimulation enhances mitochondrial biogenesis, which supports the potential
288 of LLE-mediated brown fat activation.

289 **3.6. β3-AR/AMPK signaling in LLE-induced thermogenesis in $C_3H_{10}T_{1/2}$ cells**

290 As shown in Fig. 5A-E. LLE stimulation induced an increase in the ratios of p-
291 AMPKα/AMPKα, p-AMPKβ1/AMPKβ1, p-ACC/ACC (a downstream signaling molecule of
292 AMPK), and p-p38/p38 (Fig. 5A-E). Furthermore, browning markers SIRT1, PGC-1α, PLIN5
293 and UCP1, which are downstream of AMPK signaling, were dose-dependently increased in
294 $C_3H_{10}T_{1/2}$ cells treated with LLE (Fig. 5F-I), indicating possible activation of AMPK by LLE.

295 For further confirmation, Com C, an AMPK inhibitor, was used to examine AMPK-regulated
296 brown fat activation. Com C markedly blocked AMPKα/β phosphorylation and UCP1 (Fig. 5J-
297 M). However, LLE (100 μg/mL) treatment partially reversed the inhibitory effect of Com C.
298 To identify that β3-AR is possibly the upstream signaling molecule of AMPK, the β3-
299 adrenergic agonist CL316243 was added. The increased p-AMPKα/AMPKα ratio and UCP1
300 protein expression were found in LLE-treated cell stimulated with CL316243 compared with
301 that in the unstimulated cells (Fig. 5N-5P), demonstrating LLE may act on β3-AR/AMPK
302 signaling in $C_3H_{10}T_{1/2}$ cells to activate brown adipocytes.

303 **3.7. β3-AR/AMPK signaling in Q3G-induced thermogenesis in $C_3H_{10}T_{1/2}$ cells**

304 As Q3G was determined to the most abundant flavonoid component of LLE, we investigated
305 its action in $C_3H_{10}T_{1/2}$ cells (concentration at 1~10 μM was chosen according to cytotoxicity
306 assay) (Fig. 6A). The relative mRNA expression levels of lipolytic genes (*Atgl* and *Plin5*),
307 mitochondrial biogenesis and brown markers, including *Sirt1*, *Ppargc1a*, *Adrb3*, *Cox-2*, *Cox7a*,
308 *PPARα*, *Nrf1* and *UCP1* were enhanced by Q3G, mainly at concentrations of at 5 and 10 μM
309 (Fig. 6B). Furthermore, immunostaining similarly demonstrated that Q3G stimulation
310 increased expression of UCP1 (Fig. 6C). MitoTracker and DCF-DA fluorescent showed Q3G
311 dose-dependently enhanced mitochondrial abundance (Fig. 6D-E) and reduced ROS levels,
312 which were comparable to that of the positive group (forskolin, an adenylyl cyclase activator
313 that can enhance mitochondrial activity and highly induce UCP1 expression *via*
314 phosphorylation of AMPK) (Hutchinson, Chernogubova, Dallner, Cannon, & Bengtsson, 2005)
315 (Fig. 6F-G). The result of oxygen consumption rate measurement also showed a growing trend

in Q3G-treated cells (Supplemental Fig. 1). The evidence above suggests that Q3G was beneficial for mitochondrial biogenesis. To determine Q3G affects $C_3H_{10}T_{1/2}$ cells *via* AMPK signaling, proteins associated with this signaling were measured by western blotting. The p-AMPKα/AMPKα ratio and UCP1, SIRT1, COX-2, and TFAM protein expression were enhanced with Q3G stimulation, and the level of response was similar to forskolin treatment. However, Com C significantly blocked the p-AMPKα/AMPKα ratio and the expression levels of SIRT1, COX-2, TFAM, and UCP1 (Fig. 6H-K). Further mechanism revealed that stimulation of Q3G-treated cell with CL316243 induced the increase in p-AMPKα/AMPKα ratio and UCP1 protein expression compared with unstimulated cells (Fig. 6L and 6M), demonstrating AMPK has a positive effect on browning induced by Q3G through the β3-AR signaling.

4. Discussion

~~Recently, mounting evidence supports that fat cell browning can increase energy expenditure, thereby reducing body weight (Hu et al., 2020). The discovery of pharmacological substances in natural products that can activate BAT and has great potential to exert a potential therapeutic approach for obesity and associated metabolic syndromes.~~ Lotus leaf contains rich polyphenol compounds affected by the cultivars, growth stages, seasons, harvest time, and treatment methods (e.g., ultrasonic, microwave, supercritical extraction) (Wang et al., 2021b). The TPC in the LLE was 383.7 mg/kg DW in our study, which approaches some previous reports (Huang et al., 2010; Lin et al., 2009). Although numerous studies have demonstrated

lotus leaves extracts combat obesity through a variety of mechanisms, whether thermogenesis in brown adipocytes is a potential therapeutic approach had not been determined. ~~*In vitro* models (e.g., mesenchymal stem cells) are considered to be critical for researchers to investigate the cell-autonomous actions of brown adipocytes (Zhang et al., 2018). Therefore, $C_3H_{10}T_{1/2}$ cells were employed to evaluate the brown-promoting effect of LLE and further understand the potential mechanism of its action~~ Strategies for brown adipocytes function may be split into two categories: facilitating brown preadipocyte differentiation and enhancing thermogenesis (Duan et al., 2020; Huang et al., 2020). ~~The *aP2* and *PPARγ and reduced* lipid droplet number and size Here, we found that the LLE stimulation did not affect the capacity of $C_3H_{10}T_{1/2}$ cells to differentiate into adipocytes as *aP2* and *PPARγ* expression was not significantly affected. However, LLE treatment resulted in the appearance of key properties intrinsically linked with the BAT lineage~~. The reduction in lipid droplet number and size induced by LLE may be due to the augmented lipolysis associated with the activation of brown adipocytes differentiated from $C_3H_{10}T_{1/2}$ cells, and therefore potentially benefit from the enhancement of brown adipocytes activity (Huang et al., 2010; Imran et al., 2017; Rahman & Kim, 2020a). ~~Indeed, significantly upregulated lipolysis-related gene and protein expressions were exhibited in LLE-stimulated cells and therefore potentially benefit from browning.~~ Typical brown fat possesses high expression of UCP1, which is responsible for the dissipation of energy (Ortega-Molina & Serrano, 2013). Furthermore, the PGC-1α, Sirt1, Plin5 and Cidea, which are widely considered as markers for the emergence of brown-like adipocytes (Cheng et al., 2022), were also drastically upregulated in the LLE-treated cells. However, it is noteworthy

358 that *Prdm16* was not affected by LLE treatment, as evidence suggests that it is dispensable for
359 brown fat development (Harms, 2015). Similarly, the *Prdm16* expression showed no change in
360 cAMP-stimulated brown fat cells (Seale et al., 2007). In short, these data suggest that LLE may
361 induce the brown phenotype in $C_3H_{10}T_{1/2}$ cells.
362 Inducible brown adipocytes have a high proportion of mitochondria and can therefore break
363 down lipids to generate heat *via* UCP1-mediated thermogenesis (Liu, Wang, & Lin, 2019). A
364 series of changes in mitochondrial metabolism, including an increase in mitochondrial numbers,
365 occurs in the transformation of $C_3H_{10}T_{1/2}$ cells to a brown adipocyte phenotype. Moreover, it
366 is generally acknowledged that mitochondrial dysfunction is related to enhanced ROS
367 generation and accompanied by altered mitochondrial membrane permeability, thus leading to
368 a loss of MMP (Smith, Soeters, Wüst, & Houtkooper, 2018). The induced increase in
369 mitochondrial abundance and MMP but decrease in ROS level suggests LLE's potential in
370 mitochondrial function. PGC-1α is thought to be a key activator of mitochondrial biogenesis,
371 which is required for the thermogenic process by inducing the downstream transcription factors,
372 for example Nrf1, Nrf2 and Tfam (Zhidan Wu et al., 1999). Furthermore, evidence suggests
373 that Adrb3α and Pparα are required for brown-specific markers expression in browning process
374 and are responsible for mitochondrial β-oxidation (Gonzalez-Hurtado, Lee, Choi, & Wolfgang,
375 2018). The findings of the present study demonstrate the potential of LLE for the maintenance
376 of mitochondrial activity and thermogenic programing.
377 AMPK acts as an energy sensor and selective deletion of the alpha/beta subunit in adipocytes
378 has demonstrated that AMPK is required for multiple processes in BAT, including

379 mitochondrial function, energy burning and brown adipocyte formation (van der Vaart et al.,
380 2021). AMPK has been proposed to activate p38 MAPK signaling, which regulates PGC-1α
381 expression and mitochondrial biogenesis (O'Neill, Holloway, & Steinberg, 2013). Previous *in*
382 *vivo* studies have reported that lotus leaves attenuated hepatic steatosis by phosphorylation of
383 AMPK, indicating that AMPK signaling is involved in LLE-regulated lipid metabolism (Wu et
384 al., 2010). Therefore, we explored whether the AMPK pathway is involved in LLE-induced
385 BAT activation. PGC-1α is a brown adipocyte marker and influenced by AMPK and Sirt1
386 through direct phosphorylation and deacetylation, respectively (Singh et al., 2016). Activation
387 of AMPK can induce Sirt1 activity by enhancing cellular NAD^+ levels, leading to BAT
388 activation (Hu et al., 2020). Moreover, PLIN5, regulated by AMPK or PPARγ activity (Han,
389 Xu, & Lin, 2019), is potentially elevated in BAT and induced following brown adipogenic
390 cocktail owing to higher expressions of PPARα and its co-regulator PGC-1α (Barneda, Frontini,
391 Cinti, & Christian, 2013). Here, we observed LLE significantly increased AMPK and p38
392 phosphorylation, and the downstream proteins SIRT1, PGC-1α and PLIN5, thereby stimulating
393 UCP1 expression. However, pretreatment with Com C lowered AMPKα/β1 phosphorylation
394 accompanied with a decrease in UCP1 expression. Therefore, LLE stimulated the activation of
395 BAT in $C_3H_{10}T_{1/2}$ cells by regulating mitochondrial biogenesis, which occurred in part through
396 AMPK signaling.
397 ~~Considerable evidence has shown that lotus leaves contain abundant flavonoids, but their~~
398 ~~profiles vary due to the differences in climatic conditions, varieties, or postharvest~~
399 ~~interventions.[9] Here, our results demonstrated that lotus leaves possessed flavonoids at~~

~~178.3μg/mg, with quercetin 3-O-glucuronide (Q3G) the most abundant (128.2 μg/mg).~~ Compelling evidence from multiple epidemiological and laboratory studies support a positive association between regular consumption of dietary flavonoids and BAT activity (Zhang et al., 2019). Of the seven flavonoids we identified, procyanidin B and rutin have been reported to have an activating effect on brown fat (Ma et al., 2021), but it was present at lowest levels (0.68% and 0.15% in LLE, respectively) in our study and may not play a major role. The highest percentage of Q3G (12.8%) was found in lotus leaf extract, which is consistent with some previous reports (Lee et al., 2020; Lin, Kuo, Lin, & Chiang, 2009; Qian, Chen, Qi, & Liu, 2018; Ye, He, Yan, & Chang, 2014), allowing us to speculate the brown-promoting effect of LLE could be mainly attributed to Q3G action. Although quercetin has been proven to upregulate UCP1, leading to elevated BAT activity (Choi, Kim, & Yu, 2018), but the actions of its conjugates had not been determined. Importantly, conjugated metabolites may possess biological properties that are different from those of the parent compound. The response to Q3G on the phosphorylation level of AMPK and its downstream targets SIRT1, COX-2, Tfam and UCP1 suggests possible involvement of the AMPK signaling in the Q3G-regulated activation of brown adipocytes.

β-adrenergic stimuli is capable of stimulating BAT thermogenesis by activating AMPK, which is responsible for mitochondrial metabolism (Mottillo et al., 2016). Evidence revealed that the treatment of CL316243, a beta3-AR agonist, increased the phosphorylation of AMPK and UCP1 level in adipocytes (Merlin et al., 2018; Ohsaka, Nishino, & Nomura, 2014). Stimulation of LLE or Q3G-treated cells with CL316243 induced phosphorylation of AMPKα and UCP1

expression, indicating β3-AR/AMPK signaling may involve in this process. Take together, our data revealed that LLE (most likely Q3G) effectively activated brown adipocytes and induced mitochondrial biogenesis *via* β3-AR/AMPK signaling. However, due to the lack of *in vivo* findings, future animal studies will be conducted to further validate this conclusion.

5. Conclusion

In conclusion, this study reveals that LLE enhanced lipolysis and induced a brown-fat gene expression signature and mitochondrial biogenesis in $C_3H_{10}T_{1/2}$ MSCs through a mechanism involving the activation of β3-AR/AMPK signaling. The browning effect of LLE may be mainly due to its high content of Q3G (Fig. 7). The findings demonstrate that lotus leaves are a promising therapeutic candidate for obesity based on their ability to enhance energy expenditure by thermogenesis in brown adipocytes.

CRediT authorship contribution statement

Zhenyu Wang: Investigation, Methodology, Visualization, Writing-original draft. Chaoyi Xue: Investigation, Methodology. Xuan Wang: Investigation, Formal analysis. MaoMao Zeng: Supervision. Zhaojun Wang: Supervision. Qiuming Chen: Supervision. Jie Chen: Supervision, Project administration; Mark Christian: Validation, review & editing. Zhiyong He: Conceptualization, Validation, Supervision, review & editing-Funding acquisition.

Declarations of competing interest

The authors declare no conflicts of interest

Acknowledgment

The authors acknowledge financial support from the National Natural Science Foundation of China (No. 31771978), the Six Talent Peaks Project in Jiangsu Province (No. NY-095), the National First-class Discipline Program of Food Science and Technology (No. JUFSTR20180201), the Innovation and Exploration Fund of State Key Laboratory of Food Science and Technology, Jiangnan University (No. SKLF-ZZB-202102) and the Fundamental Research Funds for the Central Universities (No. JUSRP21802).

References

Barneda, D., Frontini, A., Cinti, S., & Christian, M. (2013). Dynamic changes in lipid droplet-associated proteins in the "browning" of white adipose tissues. *Biochimica et Biophysica Acta (BBA) - Molecular and Cell Biology of Lipids, 1831* (5), 924-933.

Cheng, L., Wang, J., An, Y., Dai, H., Duan, Y., Shi, L., Lv, Y., Li, H., Wang, C., & Du, H. J. B. J. o. N. (2022). Mulberry leaf activates brown adipose tissue and induces browning of inguinal white adipose tissue in type 2 diabetic rats through regulating AMP-activated

protein kinase signalling pathway. *British Journal of Nutrition*, 127(6), 810-822.

Cheng, Y., Quan, W., Qu, T., He, Y., Wang, Z., Zeng, M., Qin, F., Chen, J., & He, Z. (2021). Effects of 60Co-irradiation and superfine grinding wall disruption pretreatment on phenolic compounds in pine (Pinus yunnanensis) pollen and its antioxidant and α-glucosidase-inhibiting activities. *Food Chemistry, 345*, 128808.

Choi, H., Kim, C.-S., & Yu, R. (2018). Quercetin Upregulates Uncoupling Protein 1 in White/Brown Adipose Tissues through Sympathetic Stimulation. *Journal of obesity & metabolic syndrome, 27* (2), 102-109.

Chou, Y.-C., Ho, C.-T., & Pan, M.-H. (2018). Immature Citrus reticulata Extract Promotes Browning of Beige Adipocytes in High-Fat Diet-Induced C57BL/6 Mice. *Journal of Agricultural and Food Chemistry, 66* (37), 9697-9703.

Deng, J., Chen, S., Yin, X., Wang, K., Liu, Y., Li, S., & Yang, P. (2013). Systematic qualitative and quantitative assessment of anthocyanins, flavones and flavonols in the petals of 108 lotus (Nelumbo nucifera) cultivars. *Food Chemistry, 139* (1-4), 307-312.

Duan, Y.-N., Ge, X., Jiang, H.-W., Zhang, H.-J., Zhao, Y., Li, J.-L., Zhang, W., & Li, J.-Y. (2020). Diphyllin Improves High-Fat Diet-Induced Obesity in Mice Through Brown and Beige Adipocytes. *Frontiers in endocrinology*,*11*, 592818.

Enerbäck, S. (2010). Human Brown Adipose Tissue. *Cell Metabolism, 11* (4), 248-252.

Giralt, M., & Villarroya, F. (2013). White, Brown, Beige/Brite: Different Adipose Cells for Different Functions? *Endocrinology, 154* (9), 2992-3000.

Gonzalez-Hurtado, E., Lee, J., Choi, J., & Wolfgang, M. J. (2018). Fatty acid oxidation is required for active and quiescent brown adipose tissue maintenance and thermogenic programing. *Molecular Metabolism, 7*, 45-56.

Guo, Y., Chen, X., Qi, J., & Yu, B. (2016). Simultaneous qualitative and quantitative analysis of flavonoids and alkaloids from the leaves of Nelumbo nucifera Gaertn. using high-performance liquid chromatography with quadrupole time-of-flight mass spectrometry. *Journal of Separation Science, 39* (13), 2499-2507.

Han, X.-q., Xu, S.-q., & Lin, J.-g. (2019). Curcumin Recovers Intracellular Lipid Droplet Formation Through Increasing Perilipin 5 Gene Expression in Activated Hepatic Stellate Cells In Vitro. *Current Medical Science, 39* (5), 766-777.

Harms, M. J. (2015). Controlling Thermogenesis: Understanding the Role of PRDM16 in the Development and Function of Brown Fat.

Hu, J., Wang, Z., Tan, B. K., & Christian, M. (2020). Dietary polyphenols turn fat “brown”: A narrative review of the possible mechanisms. *Trends in Food Science & Technology, 97*, 221-232.

Huang, B., Ban, X., He, J., Tong, J., Tian, J., & Wang, Y. (2010). Hepatoprotective and antioxidant activity of ethanolic extracts of edible lotus (Nelumbo nucifera Gaertn.) leaves. *Food Chemistry, 120* (3), 873-878.

Huang, Y., Wei, G., Peng, X., Hu, G., Su, H., Liu, J., Chen, X., & Qiu, M. (2020). Triterpenoids from functional mushroom Ganoderma resinaceum and the novel role of Resinacein S in enhancing the activity of brown/beige adipocytes. *Food Research International, 136*, 109303.

Hutchinson, D. S., Chernogubova, E., Dallner, O. S., Cannon, B., & Bengtsson, T. J. D. (2005). β-Adrenoceptors, but not α-adrenoceptors, stimulate AMP-activated protein kinase in brown adipocytes independently of uncoupling protein-1. *Diabetologia*, *48* (11), 2386-2395.

Imran, K. M., Rahman, N., Yoon, D., Jeon, M., Lee, B.-T., & Kim, Y.-S. (2017). Cryptotanshinone promotes commitment to the brown adipocyte lineage and mitochondrial biogenesis in C3H10T1/2 mesenchymal stem cells via AMPK and p38-MAPK signaling. *Biochimica et Biophysica Acta (BBA) - Molecular and Cell Biology of Lipids, 1862* (10, Part A), 1110-1120.

Lee, J. S., Paje, L. A., Choi, W.-H., Cho, E. J., Kim, H. Y., Jacinto, S. D., & Lee, S. (2020). Validation of an optimized HPLC/UV method for the quantification of flavonoids in lotus. *Applied Biological Chemistry, 63* (1), 84.

Limwachiranon, J., Huang, H., Shi, Z., Li, L., & Luo, Z. (2018). Lotus Flavonoids and Phenolic Acids: Health Promotion and Safe Consumption Dosages. *Comprehensive Reviews in Food Science and Food Safety*, 17 (2), 458-471.

Lin, H.-Y., Kuo, Y.-H., Lin, Y.-L., & Chiang, W. (2009). Antioxidative Effect and Active Components from Leaves of Lotus (Nelumbo nucifera). *Journal Of Agricultural And Food Chemistry, 57* (15), 6623-6629.

Lin, M.-C., Kao, S.-H., Chung, P.-J., Chan, K.-C., Yang, M.-Y., & Wang, C.-J. (2009). Improvement for High Fat Diet-Induced Hepatic Injuries and Oxidative Stress by Flavonoid-Enriched Extract from Nelumbo nucifera Leaf. *Journal of Agricultural and Food Chemistry, 57* (13), 5925-5932.

Liu, J., Wang, Y., & Lin, L. (2019). Small molecules for fat combustion: targeting obesity. *Acta Pharmaceutica Sinica B, 9* (2), 220-236.

Ma, B., Hao, J., Xu, H., Liu, L., Wang, W., Chen, S., & Wu, H. (2022). Rutin promotes white adipose tissue "browning" and brown adipose tissue activation partially through the calmodulin-dependent protein kinase kinase β/AMP-activated protein kinase pathway. *Endocrine Journal, 69*(4), 385-397.

Merlin, J., Sato, M., Chia, L. Y., Fahey, R., Pakzad, M., Nowell, C. J., Summers, R. J., Bengtsson, T., Evans, B. A., & Hutchinson, D. S. J. F. i. e. (2018). Rosiglitazone and a β3-adrenoceptor agonist are both required for functional browning of white adipocytes in culture. *Frontiers in Endocrinology*, *9*, 249.

Mottillo, Emilio P., Desjardins, Eric M., Crane, Justin D., Smith, Brennan K., Green, Alex E., Ducommun, S., Henriksen, Tora I., Rebalka, Irena A., Razi, A., Sakamoto, K., Scheele, C., Kemp, Bruce E., Hawke, Thomas J., Ortega, J., Granneman, James G., & Steinberg, Gregory R. (2016). Lack of Adipocyte AMPK Exacerbates Insulin Resistance and Hepatic Steatosis through Brown and Beige Adipose Tissue Function. *Cell Metabolism, 24* (1), 118-129.

Ohsaka, Y., Nishino, H., & Nomura, Y. (2014). Adipose cells induce phospho-Thr-172 AMPK production by epinephrine or CL316243 in mouse 3T3-L1 adipocytes or MAPK activation and G protein-associated PI3K responses induced by CL316243 or aluminum fluoride in rat white adipocytes. *Folia Biologica,60* (4), 168.

O'Neill, H. M., Holloway, G. P., & Steinberg, G. R. (2013). AMPK regulation of fatty acid metabolism and mitochondrial biogenesis: Implications for obesity. *Molecular And Cellular Endocrinology, 366* (2), 135-151.

Ortega-Molina, A., & Serrano, M. (2013). PTEN in cancer, metabolism, and aging. *Trends in endocrinology and metabolism: TEM, 24* (4), 184-189.

Qian, Y., Chen, X., Qi, J., & Liu, X. (2018). A novel analytical method based on HPLC-PDA coupled post-column derivatization to evaluate the ability to inhibit tyrosine nitration in lotus leaf extracts. *RSC Advances, 8* (68), 38715-38720.

Rahman, M. S., & Kim, Y.-S. (2020a). Mangiferin induces the expression of a thermogenic signature via AMPK signaling during brown-adipocyte differentiation. *Food And Chemical Toxicology, 141*, 111415.

Rahman, M. S., & Kim, Y.-S. (2020b). PINK1–PRKN mitophagy suppression by mangiferin promotes a brown-fat-phenotype via PKA-p38 MAPK signalling in murine C3H10T1/2 mesenchymal stem cells. *Metabolism-clinical and Experimental, 107*, 154228.

Sanhueza, E., Paredes-Osses, E., González, C. L., & García, A. (2015). Effect of pH in the survival of Lactobacillus salivarius strain UCO_979C wild type and the pH acid acclimated variant. *Electronic Journal of Biotechnology, 18* (5), 343-346.

Seale, P., Kajimura, S., Yang, W., Chin, S., Rohas, L. M., Uldry, M., Tavernier, G., Langin, D., & Spiegelman, B. M. (2007). Transcriptional Control of Brown Fat Determination by PRDM16. *Cell Metabolism, 6* (1), 38-54.

Sharma, R., Matsuzaka, T., Kaushik, M. K., Sugasawa, T., Ohno, H., Wang, Y., Motomura, K., Shimura, T., Okajima, Y., Mizunoe, Y., Ma, Y., Saber, Z. M., Iwasaki, H., Yatoh, S., Suzuki, H., Aita, Y., Han, S.-I., Takeuchi, Y., Yahagi, N., Miyamoto, T., Sekiya, M., Nakagawa, Y., & Shimano, H. (2019). Octacosanol and policosanol prevent high-fat diet-induced obesity and metabolic disorders by activating brown adipose tissue and improving liver metabolism. *Scientific Reports, 9* (1), 5169-5169.

Sim, W.-S., Choi, S.-I., Cho, B.-Y., Choi, S.-H., Han, X., Cho, H.-D., Kim, S.-H., Lee, B.-Y., Kang, I.-J., Cho, J.-H., & Lee, O.-H. (2019). Anti-Obesity Effect of Extract from Nelumbo Nucifera L., Morus Alba L., and Raphanus Sativus Mixture in 3T3-L1 Adipocytes and C57BL/6J Obese Mice. *Foods*, *8* (5), 170.

Singh, S. P., Bellner, L., Vanella, L., Cao, J., Falck, J. R., Kappas, A., & Abraham, N. G. (2016). Downregulation of PGC-1α Prevents the Beneficial Effect of EET-Heme Oxygenase-1 on Mitochondrial Integrity and Associated Metabolic Function in Obese Mice. *Journal of Nutrition and Metabolism, 2016*, 9039754-9039754.

Smith, R. L., Soeters, M. R., Wüst, R. C. I., & Houtkooper, R. H. (2018). Metabolic Flexibility as an Adaptation to Energy Resources and Requirements in Health and Disease. *Endocrine Reviews, 39* (4), 489-517.

Song, J., Kim, J., Park, H. J., & Kim, H. (2020). Anti-Obesity Effects of a Prunus persica and Nelumbo nucifera Mixture in Mice Fed a High-Fat Diet. *Nutrients*, *12* (11), 3392.

Tao, Y., Chen, Z., Zhang, Y., Wang, Y., & Cheng, Y. (2013). Immobilized magnetic beads based multi-target affinity selection coupled with high performance liquid chromatography–mass spectrometry for screening anti-diabetic compounds from a Chinese medicine

"Tang-Zhi-Qing". *Journal of Pharmaceutical and Biomedical Analysis, 78-79*, 190-201.

van der Vaart, J. I., Boon, M. R., & Houtkooper, R. H. (2021). The Role of AMPK Signaling in Brown Adipose Tissue Activation. *Cells*, *10* (5), 1122.

Wang, S., Pan, M. H., Hung, W. L., Tung, Y. C., & Ho, C. T. (2019). From white to beige adipocytes: therapeutic potential of dietary molecules against obesity and their molecular mechanisms. *Food & Function, 10* (3), 1263-1279.

Wang, X., Chen, J., Rong, C., Pan, F., Zhao, X., Hu, Y. (2018). GLP-1RA promotes brown adipogenesis of C3H10T1/2 mesenchymal stem cells via the PI3K-AKT-mTOR signaling pathway. *Biochemical and Biophysical Research Communications*, *506* (4), 976-982.

Wang, Z., Cheng, Y., Zeng, M., Wang, Z., Qin, F., Wang, Y., Chen, J., He, Z. (2021a). Lotus (Nelumbo nucifera Gaertn.) leaf: A narrative review of its Phytoconstituents, health benefits and food industry applications. *Trends in Food Science & Technology*, *112*, 631-650.

Wang, Z., Hu, J., Hamzah, S. S., Ge, S., Lin, Y., Zheng, B., Zeng, S., & Lin, S. (2019). n-Butanol Extract of Lotus Seeds Exerts Antiobesity Effects in 3T3-L1 Preadipocytes and High-Fat Diet-Fed Mice via Activating Adenosine Monophosphate-Activated Protein Kinase. *Journal of Agricultural and Food Chemistry, 67* (4), 1092-1103.

Wang, Z., Zeng, M., Wang, Z., Qin, F., Wang, Y., Chen, J., Christian, M., & He, Z. (2021b). Food phenolics stimulate adipocyte browning via regulating gut microecology. *Critical Reviews in Food Science and Nutrition*, 1-27.

Wu, C.-H., Yang, M.-Y., Chan, K.-C., Chung, P.-J., Ou, T.-T., & Wang, C.-J. (2010). Improvement in High-Fat Diet-Induced Obesity and Body Fat Accumulation by a Nelumbo nucifera Leaf Flavonoid-Rich Extract in Mice. *Journal of Agricultural and Food Chemistry, 58* (11), 7075-7081.

Wu, Z., Li, Y., Xu, Y., Zhang, Y., Tao, G., Zhang, L., & Shi, G. (2022). Transcriptome Analysis of Bacillus licheniformis for Improving Bacitracin Production. *ACS Synthetic Biology, 11* (3), 1325-1335.

Wu, Z., Puigserver, P., Andersson, U., Zhang, C., Adelmant, G., Mootha, V., Troy, A., Cinti, S., Lowell, B., Scarpulla, R. C., & Spiegelman, B. M. (1999). Mechanisms Controlling Mitochondrial Biogenesis and Respiration through the Thermogenic Coactivator PGC-1. *Cell, 98* (1), 115-124.

Ye, L.-H., He, X.-X., Yan, M.-Z., & Chang, Q. (2014). Identification of in vivo components in rats after oral administration of lotus leaf flavonoids using ultra fast liquid chromatography with tandem mass spectrometry. *Analytical Methods, 6* (15), 6088-6094.

Yue, L., Zhao, W., Wang, D., Meng, M., Zheng, Y., Li, Y., Qiu, J., Yu, J., Yan, Y., Lu, P., Sun, Y., Fu, J., Wang, J., Zhang, Q., Xu, L., & Ma, X. (2019). Silver nanoparticles inhibit beige fat function and promote adiposity. *Molecular Metabolism, 22*, 1-11.

Zhang, C., Deng, J., Liu, D., Tuo, X., Xiao, L., Lai, B., Yao, Q., Liu, J., Yang, H., & Wang, N. (2018). Nuciferine ameliorates hepatic steatosis in high-fat diet/streptozocin-induced diabetic mice through a PPARα/PPARγ coactivator-1α pathway. *British Journal of*

Pharmacology, 175 (22), 4218-4228.

Zhang, Z., Zhang, H., Li, B., Meng, X., Wang, J., Zhang, Y., Yao, S., Ma, Q., Jin, L., Yang, J., Wang, W., & Ning, G. (2014). Berberine activates thermogenesis in white and brown adipose tissue. *Nature Communications, 5* (1), 5493.

Zhu, M., Liu, T., Zhang, C., & Guo, M. (2017). Flavonoids of Lotus (Nelumbo nucifera) Seed Embryos and Their Antioxidant Potential. *Journal of Food Science, 82* (8), 1834-1841.

Zhu, M. Z., Wu, W., Jiao, L. L., Yang, P. F., & Guo, M. Q. (2015). Analysis of Flavonoids in Lotus (Nelumbo nucifera) Leaves and Their Antioxidant Activity Using Macroporous Resin Chromatography Coupled with LC-MS/MS and Antioxidant Biochemical Assays. *Molecules, 20* (6), 10553-10565.

645 **Table 1**. Identification of flavonoids in lotus leaf by UPLC-MS/MS.

Peak No.	Rt (min)	$[M-H]^-$ (m/z)	Fragment ions (m/z)	Identification	References	Contents (μg/mg)
A	3.27	577	289	procyanidin B2	(Guo, Chen, Qi, & Yu, 2016; Tao, Chen, Zhang, Wang, & Cheng, 2013)	6.86±0.44
B	4.58	595	300	quercetin 3-O-arabinopyranosyl-(1→2)-galactopyranoside	(Deng et al., 2013)	12.95±0.82
C	4.91	609	300, 301	rutin	(Zhu, Liu, Zhang, & Guo, 2017)	1.52±0.10
D	5.13	477	301	quercetin 3-O-glucuronide	(Deng et al., 2013; Zhu et al., 2017); standard	128.21±8.16
E	5.66	447	285	kaempferol 3-O-glucoside	(Ye et al., 2014)	5.48±0.35
F	6.86	623	314, 315	isorhamnetin 3-O-rutinoside	(Deng et al., 2013; Zhu et al., 2017)	0.52±0.03
G	7.37	477	314	isorhamnetin 3-O-glucoside	(Deng et al., 2013; Zhu, Wu, Jiao, Yang, & Guo, 2015)	3.51±0.22

646 Note: all quantified as quercetin 3-O-glucuronide

647

648

649

650 **Table 2.** Primer sequences for RT-PCR used in $C_3H_{10}T_{1/2}$ cells.

Target genes	Forward primer sequence (5′ to 3′)	Reverse primer sequence (5′ to 3′)
β-actin	5'–GTGCTATGTTGCTCTAGACTTCG-3'	5'–ATGCCACAGGATTCCATACC-3'
Pparγ	5'–AGAACCTGCATCTCCACCTTAT-3'	5'-CCACAGACTCGGCACTCAAT-3'
C/ebpα	5'-GAGGCTCACCTTCACATCTTTC-3'	5'-CTCTGTCTCCTACCACATGGCT-3'
Fabp4	5'-GATGCCTTTGTGGGAACCT-3'	5'-GTTTGAAGGAAATCTCGGTGTT-3'
Ppargc1a	5'-ACAGCTTTCTGGGTGGATT-3'	5'-TGAGGACCGCTAGCAAGTTT-3'
Prdm16	5'-GAAGTCACAGGAGGACACGG-3'	5'-CTCGCTCCTCAACACACCTC-3'
Cidea	5'-TGCTCTTCTGTATCGCCCAGT-3'	5'-GCCGTGTAAGGAATCTGCTG-3'
Tfam	5'-GCAGCAGGCACTACAGCGATAC-3'	5'-TTCCCATTCCCTTCCCAGACTGAG-3'
Adrb3	5'-TGGAGTAGAGGGATGCGGGAATG-3'	5'-CAAGCACTGGAAGGAAGAGGGAAG-3'
Pparα	5'-ACATTGTGTAATCCTGGTGGTGGTG-3'	5'-CTGGCTGTCCTGGAACTTGCTATG-3'
Cox2	5'-CATGAGCCGTCCCCTCACTAGG-3'	5'-AATCCTGGTCGGTTTGATGCTACTG-3'
Cox7a	5'-CCACTGGCTTGCTCTGGTCATAAG-3'	5'-CTGGCTATCTTGGAACTCACTCTGC-3'

Sirt1	5'-GCATAGATACCGTCTCTTGATCTGAA-3'	5'-TGTGAAGTTACTGCAGGAGTGTAAA-3'
Ucp1	5'-GGCATTCAGAGGCAAATCAGCT-3'	5'-CAATGAACACTGCCACACCTC-3'
Nrf1	5'-CCACGTTGGATGAGTACACG-3'	5'-CAGACTCGAGGTCTTCCAGG-3'
Atgl	5'-CAACGCCACTCACATCTACGG-3'	5'-GGACACCTCAATAATGTTGGCAC-3'
Hsl	5'-CCAGCCTGAGGGCTTACTG-3'	5'-CTCCATTGACATCTCG-3'
Abhd5	5'-TGACAGTGATGCGGAAGAAG-3'	5'-AGATCTGGTCGCTCAGGAAA-3'
Plin1	5'-GGCTCTGGGAAGCATCGA-3'	5'-GGCCTTGGGAGCCTTCTG-3'
Cpt1α	5'-CTCCGCCTGAGCCATGAAG-3'	5'-CACCAGTGATGCCATTCT-3'
Plin5	5'-TCCTGCCCGTCAAAGGGATCTGA-3'	5'-GGACATTCTGCTGTGTGGCGCT-3'

654 **Figure Legends**

655 **Fig. 1.** UPLC chromatogram of LLE (284 nm). The components appeared at the peaks A
656 (procyanidin B2), B (quercetin 3-O-arabinopyranosyl-(1→2)-galactopyranoside), C (rutin), D
657 (quercetin 3-O-glucuronide), E (kaempferol 3-O-glucoside), F (isorhamnetin 3-O-rutinoside),
658 and G (isorhamnetin 3-O-glucoside) were identified, respectively, by comparing their MS and
659 MS^2 fragmentation ions.

660 **Fig. 2.** Cytotoxicity of LLE and its effect on lipolysis. (A) The cytotoxicity of LLE on
661 c3H10T1/2 cells was determined was determined by CCK-8 assay. (B) Expression of genes
662 related to differentiation into brown adipocytes were assessed by qRT-PCR. (C and D)
663 $C_3H_{10}T_{1/2}$ cells were observed in FITC/DAPI field (cells were stained with Bodipy/DAPI
664 fluorescent dyes) and bright field, respectively (×200). (E-G) Expression of factors related to
665 lipolysis were measured by qRT-PCR and western blotting.

666 **Fig. 3**. The effect of LLE on browning-related factors in $C_3H_{10}T_{1/2}$ cells. (A) The mRNA
667 expressions of *Ucp1*, *Ppargc1a*, *Cidea*, *Prdm16*, *Sirt1*, and *Plin5* were determined by qRT-
668 PCR. Immunofluorescence analysis of SIRT1 (B and D) and UCP1 (C and E) (×400).

669 **Fig. 4**. The effect of LLE on mitochondrial biogenesis in $C_3H_{10}T_{1/2}$ cells. (A) Mitochondria
670 abundance was assessed by MitoTracker Green staining and (B) quantified (×200). (C)
671 Intracellular ROS was assessed by the DCF-DA assay and (D) quantified (×200). (E) MMP
672 levels (the ratio of polymer to monomer JC-1) were evaluated through fluorescence analysis
673 (×200) (F). (G) The mRNA expressions of *Tfam, Nrf1, Pparα*, *Adrb3*, *Cox7a*, and *Cox-2* were
674 determined by qRT-PCR. (H) Protein expressions of NRF2, TFAM, COX-2, and COX-IV were

675 measured by western blotting.

676 **Fig. 5.** Effect of LLE on the β3-AR/AMPK signaling in $C_3H_{10}T_{1/2}$ cells. (A-I) The protein
677 expressions of (p)AMPKα/β1, (p)ACC, (p)p-38, SIRT1, PGC-1α, PLIN5, and UCP1 were
678 measured by western blotting. (J-M) The protein expressions of (p)AMPKα/β1 and UCP1 in
679 LLE (100 μg/mL)-treated $C_3H_{10}T_{1/2}$ cells with or without Com C. (N-P) The protein
680 expressions of (p)AMPKα and UCP1 in LLE (100 μg/mL)-treated cells with or without
681 CL316243.

682 **Fig. 6.** Effect of Q3G on the AMPK signaling in $C_3H_{10}T_{1/2}$ cells. (A) The cytotoxicity of Q3G
683 on $C_3H_{10}T_{1/2}$ cells. (B) The mRNA expressions of *Atgl*, *Plin5*, *Sirt1*, *Ppargc1a*, *Adrb3*, *Cox-2*,
684 *Cox7a*, *Pparα*, *Nrf1* and *Ucp1* in $C_3H_{10}T_{1/2}$ cells treated with Q3G (1, 5 and 10μM). (C)
685 Immunofluorescence analysis of UCP1 (×200). (D-E) Mitochondria abundance in Q3G or
686 forskolin (10μM)-treated cells was assessed and analysed by MitoTracker Green staining and
687 Image J, respectively. (F-G) Intracellular ROS in Q3G or forskolin (10μM)-treated cells was
688 assessed and analysed by the DCF-DA assay and Image J, respectively. (H-K) The protein
689 expressions of (p)AMPKα, UCP1, SIRT1, COX2, and TFAM in forskolin (10μM) or Q3G (5
690 and 10μM)-treated $C_3H_{10}T_{1/2}$ cells stimulated with or without Com C were determined and
691 analysed by Image J. (L and M) The protein expressions of (p)AMPKα and UCP1 in Q3G
692 (10μM)-treated cells with or without CL316243.

693 **Fig. 7.** Possible mechanism of the thermogenesis-promoting effect of Q3G-riched LLE in
694 $C_3H_{10}T_{1/2}$ cells.

Fig. 1

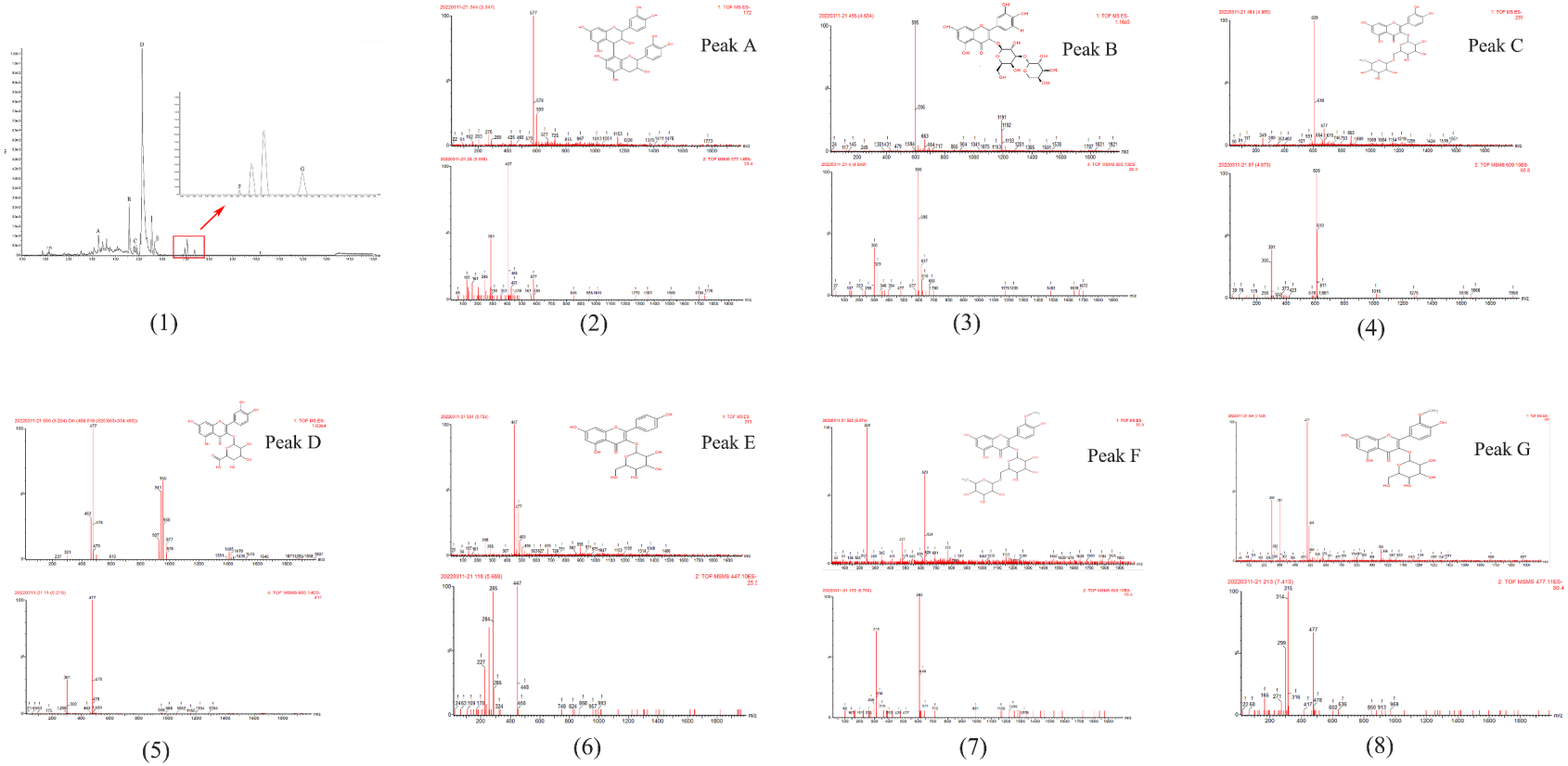

Fig. 2

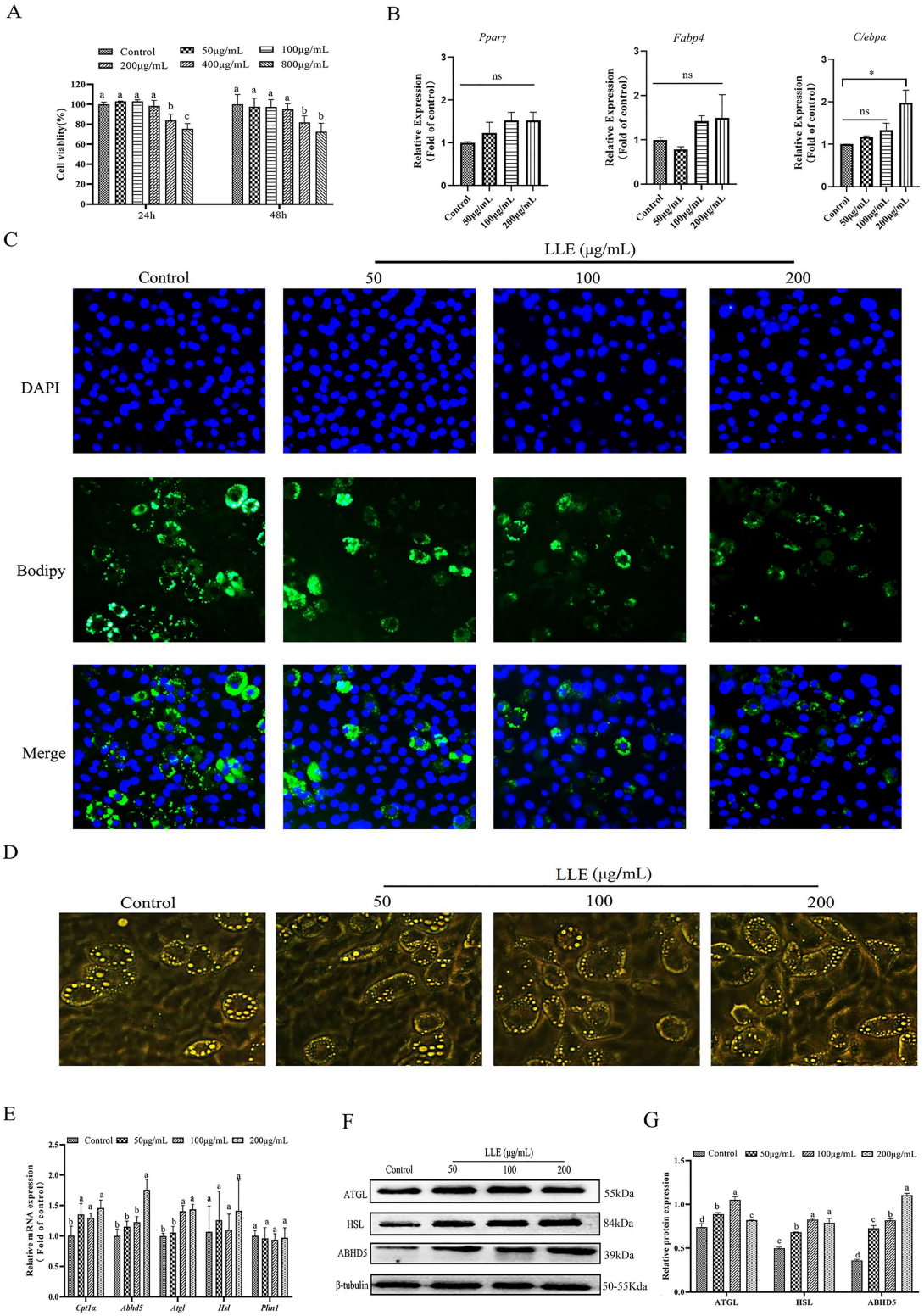
A
Control
50μg/mL
100μg/mL
200μg/mL
400μg/mL
800μg/mL
Cell viability(%)
24h
48h
B
Pparγ
Fabp4
C/ebpα
Relative Expression (Fold of control)
ns
*
Control
50μg/mL
100μg/mL
200μg/mL
C
LLE (μg/mL)
Control
50
100
200
DAPI
Bodipy
Merge
D
LLE (μg/mL)
Control
50
100
200
E
Control
50μg/mL
100μg/mL
200μg/mL
Relative mRNA expression (Fold of control)
Cpt1a
Abhd5
Atgl
Hsl
Plin1
F
LLE (μg/mL)
Control
50
100
200
ATGL
HSL
ABHD5
β-tubulin
55kDa
84kDa
39kDa
50-55Kda
G
Control
50μg/mL
100μg/mL
200μg/mL
Relative protein expression
ATGL
HSL
ABHD5

Fig. 3

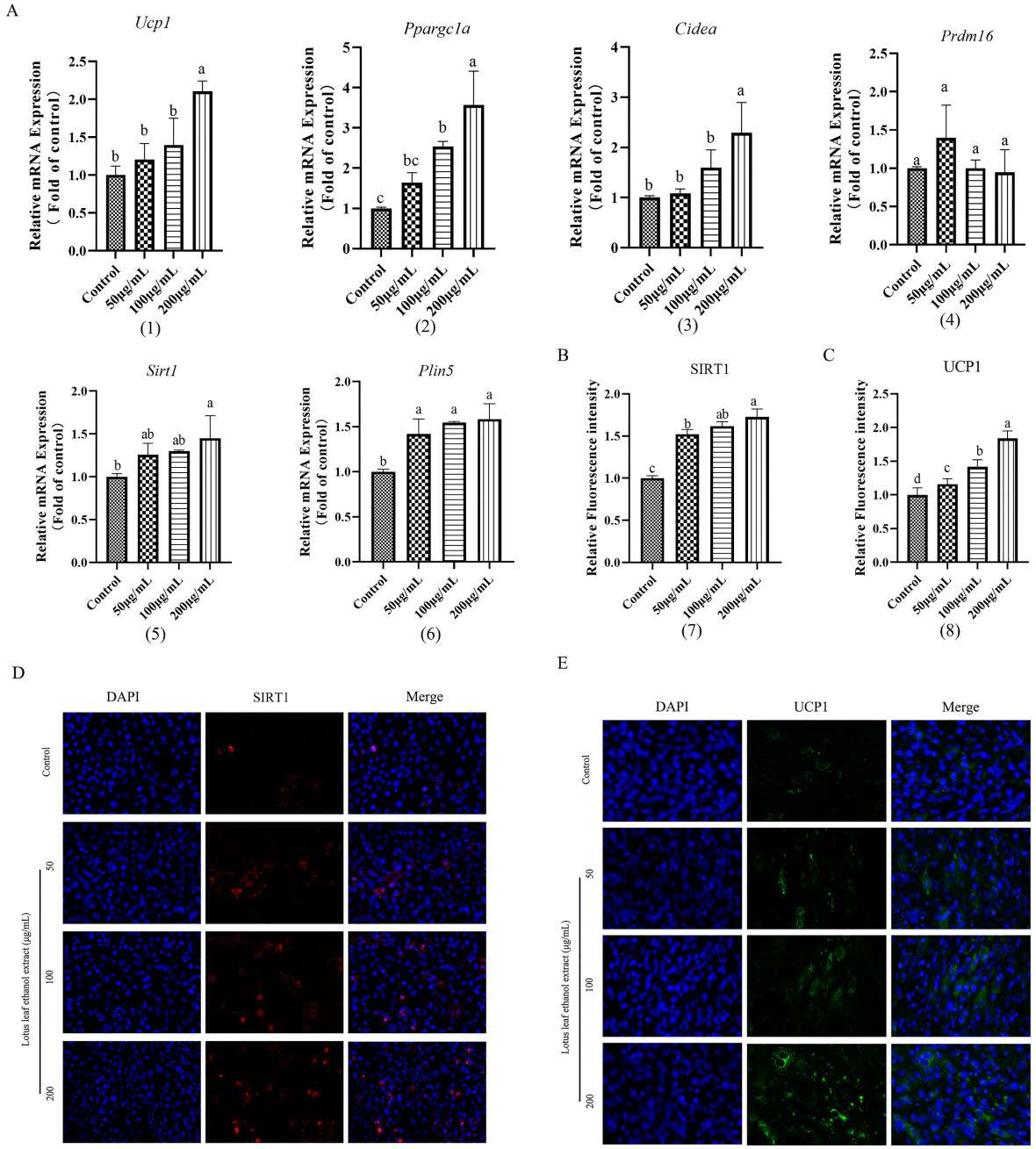
A
Ucp1
Ppargc1a
Cidea
Prdm16
Sirt1
Plin5
Relative mRNA Expression (Fold of control)
Control
50μg/mL
100μg/mL
200μg/mL
(1)
(2)
(3)
(4)
(5)
(6)
B
SIRT1
Relative Fluorescence intensity
(7)
C
UCP1
(8)
D
DAPI
SIRT1
Merge
Control
Lotus leaf ethanol extract (μg/mL)
50
100
200
E
DAPI
UCP1
Merge

Fig. 4

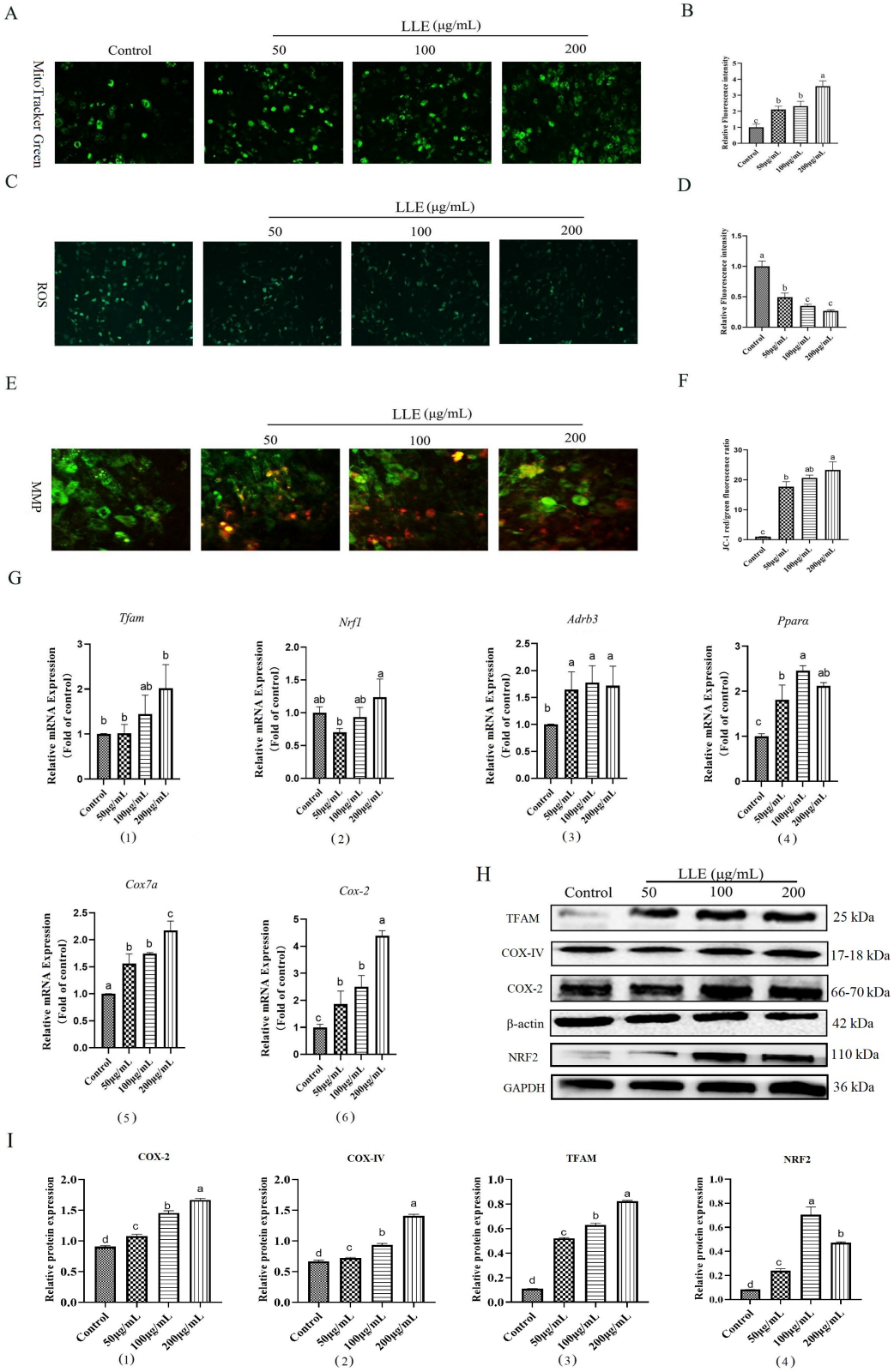
A
LLE (μg/mL)
Control
50
100
200
MitoTracker Green
B
Relative Fluorescence intensity
Control
50μg/mL
100μg/mL
200μg/mL
C
LLE (μg/mL)
50
100
200
ROS
D
Relative Fluorescence intensity
E
LLE (μg/mL)
50
100
200
MMP
F
JC-1 red/green fluorescence ratio
G
Tfam
Nrf1
Adrb3
Pparα
Cox7a
Cox-2
Relative mRNA Expression (Fold of control)
(1)
(2)
(3)
(4)
(5)
(6)
H
LLE (μg/mL)
Control
50
100
200
TFAM
COX-IV
COX-2
β-actin
NRF2
GAPDH
25 kDa
17-18 kDa
66-70 kDa
42 kDa
110 kDa
36 kDa
I
COX-2
COX-IV
TFAM
NRF2
Relative protein expression
(1)
(2)
(3)
(4)

Fig. 5

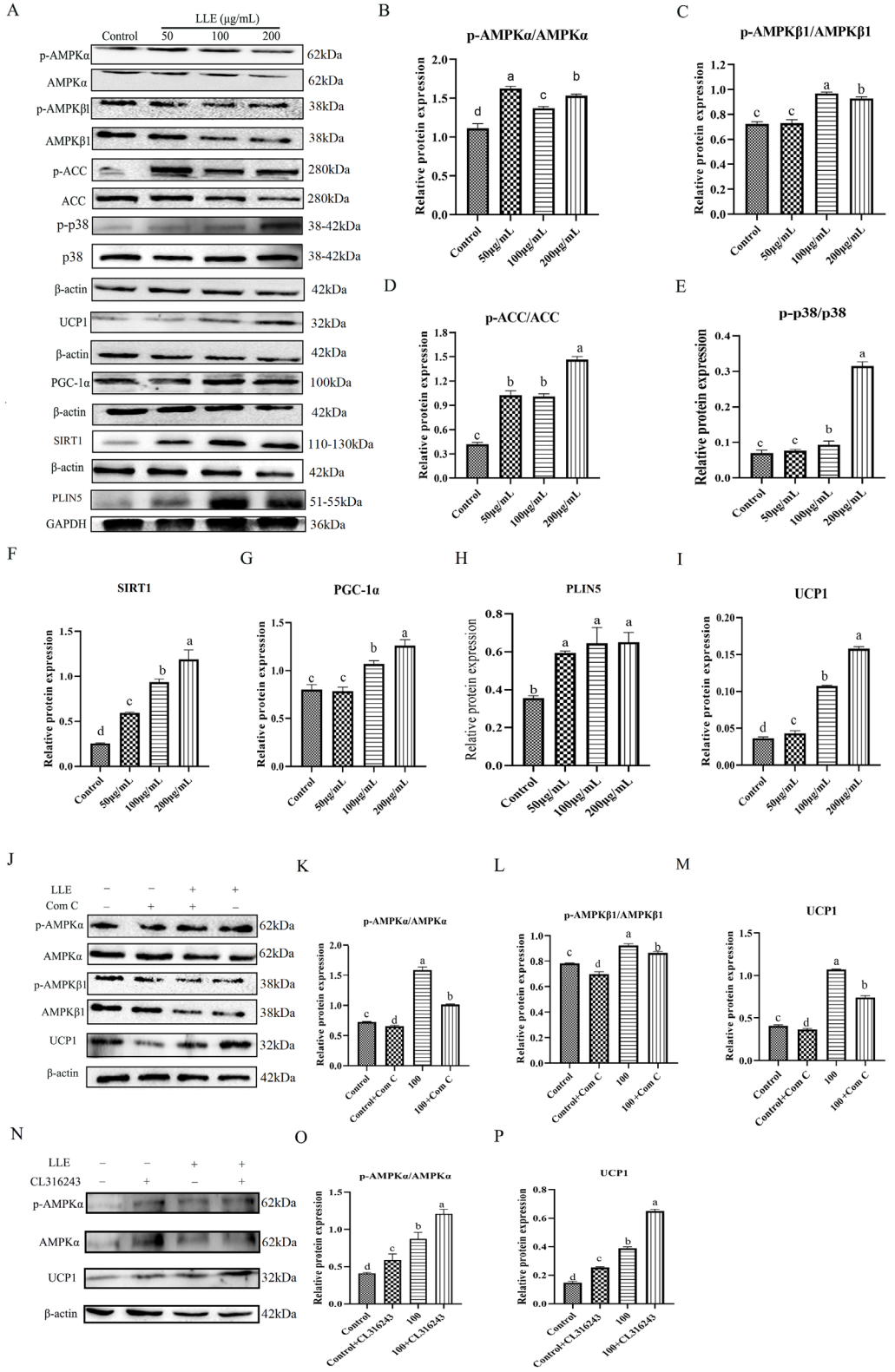
A
LLE (μg/mL)
Control
50
100
200
p-AMPKα
AMPKα
p-AMPKβ1
AMPKβ1
p-ACC
ACC
p-p38
p38
β-actin
UCP1
PGC-1α
SIRT1
PLIN5
GAPDH
62kDa
38kDa
280kDa
38-42kDa
42kDa
32kDa
100kDa
110-130kDa
51-55kDa
36kDa
B
p-AMPKα/AMPKα
C
p-AMPKβ1/AMPKβ1
D
p-ACC/ACC
E
p-p38/p38
F
SIRT1
G
PGC-1α
H
PLIN5
I
UCP1
Relative protein expression
Control
50μg/mL
100μg/mL
200μg/mL
J
LLE
Com C
K
L
M
Control+Com C
100
100+Com C
N
CL316243
O
P
Control+CL316243
100+CL316243

Fig. 6

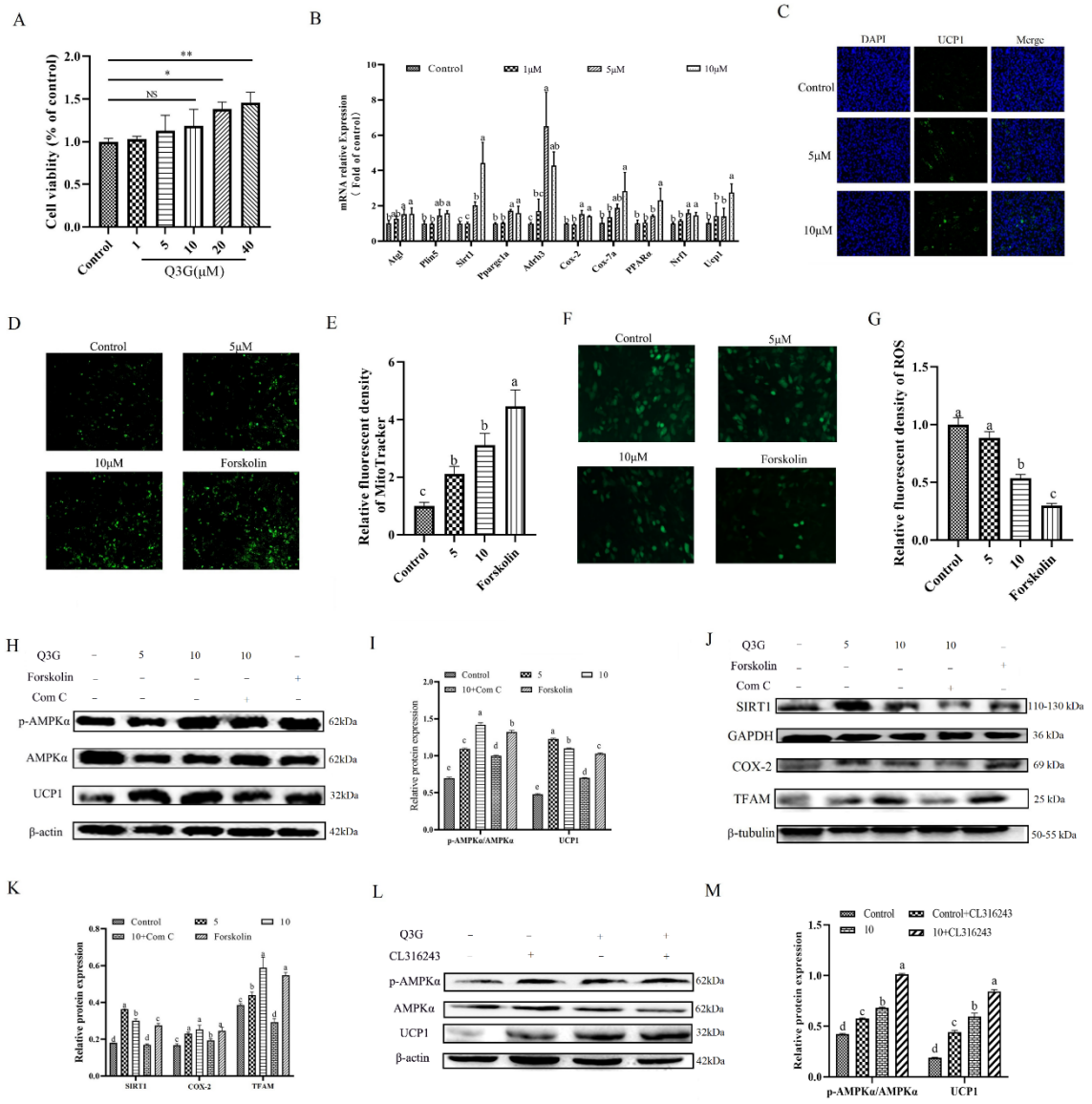
A
Cell viability (% of control)
Control
1
5
10
20
40
Q3G(μM)
B
mRNA relative Expression (Fold of control)
Control
1μM
5μM
10μM
Atg5
Pink5
Sirt1
Ppargc1a
Adrb3
Cox-2
Cox-7a
PPARα
Nrf1
Ucp1
C
DAPI
UCP1
Merge
Control
5μM
10μM
D
Control
5μM
10μM
Forskolin
E
Relative fluorescent density of MitoTracker
Control
5
10
Forskolin
F
Control
5μM
10μM
Forskolin
G
Relative fluorescent density of ROS
Control
5
10
Forskolin
H
Q3G
Forskolin
Com C
p-AMPKα
AMPKα
UCP1
β-actin
62kDa
62kDa
32kDa
42kDa
I
Control
5
10
10+Com C
Forskolin
Relative protein expression
p-AMPKα/AMPKα
UCP1
J
Q3G
Forskolin
Com C
SIRT1
GAPDH
COX-2
TFAM
β-tubulin
110-130 kDa
36 kDa
69 kDa
25 kDa
50-55 kDa
K
Control
5
10
10+Com C
Forskolin
Relative protein expression
SIRT1
COX-2
TFAM
L
Q3G
CL316243
p-AMPKα
AMPKα
UCP1
β-actin
62kDa
62kDa
32kDa
42kDa
M
Control
Control+CL316243
10
10+CL316243
Relative protein expression
p-AMPKα/AMPKα
UCP1

Fig. 7

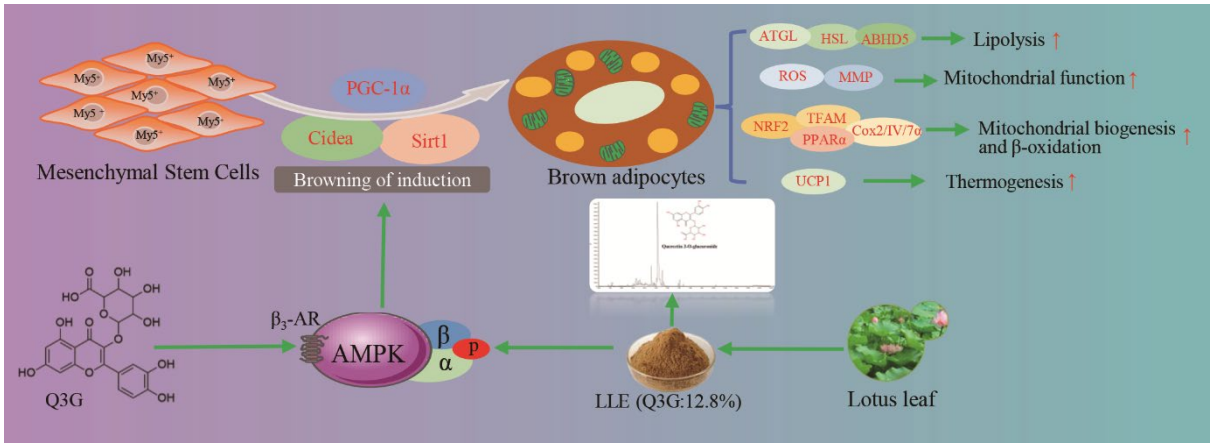
Mesenchymal Stem Cells
PGC-1α
Cidea
Sirt1
Browning of induction
Brown adipocytes
ATGL
HSL
ABHD5
Lipolysis ↑
ROS
MMP
Mitochondrial function ↑
NRF2
TFAM
PPARα
Cox2/IV/7α
Mitochondrial biogenesis and β-oxidation ↑
UCP1
Thermogenesis ↑
Q3G
β3-AR
AMPK
β
α
P
LLE (Q3G:12.8%)
Lotus leaf